Earthquakes and Structures, *Vol. 18, No. 2 (2020) 249-261*
DOI: https://doi.org/10.12989/eas.2020.18.2.249

Derivation of analytical fragility curves using SDOF models of masonry structures in Erzincan (Turkey)

Shaghayegh Karimzadeh*, Koray Kadas[a], Aysegul Askan[b], M. Altug Erberik[b] and Ahmet Yakut[b]

Department of Civil Engineering, Middle East Technical University, Üniversiteler Mahallesi, Dumlupınar Bulvarı No:1, 06800, Ankara, Turkey

(Received January 24, 2019, Revised September 13, 2019, Accepted January 4, 2020)

Abstract. Seismic loss estimation studies require fragility curves which are usually derived using ground motion datasets. Ground motion records can be either in the form of recorded or simulated time histories compatible with regional seismicity. The main purpose of this study is to investigate the use of alternative ground motion datasets (simulated and real) on the fragility curves. Simulated dataset is prepared considering regional seismicity parameters corresponding to Erzincan using the stochastic finite-fault technique. In addition, regionally compatible records are chosen from the NGA-West2 ground motion database to form the real dataset. The paper additionally studies the effects of hazard variability and two different fragility curve derivation approaches on the generated fragility curves. As the final step for verification purposes, damage states estimated for the fragility curves derived using alternative approaches are compared with the observed damage levels from the 1992 Erzincan (Turkey) earthquake (Mw=6.6). In order to accomplish all these steps, a set of representative masonry buildings from Erzincan region are analyzed using simplified structural models. The results reveal that regionally simulated ground motions can be used alternatively in fragility analyses and damage estimation studies.

Keywords: real records; simulated records; masonry structures; fragility curves; sensitivity analysis

1. Introduction

Decision makers need reliable information corresponding to the consequences of potential seismic events and this information could be assessed via accurately performed seismic risk analysis. Seismic risk analysis inherently requires fragility functions to be used in vulnerability assessment phase. Numerically or analytically-derived fragility curves are highly affected by the characteristics of the ground motion database formed. For earthquake-prone zones with sparse or no seismic monitoring network, lack of ground motion records from potential large events is disincentive to formation of reliable ground motion database. This issue could be alternatively overcome using simulated ground motions compatible with the regional characteristics of the seismic area of interest.

The majority of the fragility curve studies have been previously performed using real ground motion records worldwide (e.g., Ansal *et al*. 2009, Ugurhan *et al*. 2011, Sørensen and Lang 2015, Gokkaya 2016, Liu *et al*. 2018, Sfahani and Guan 2018). A number of these studies focus on the fragility analysis for masonry buildings (e.g., Erberik 2008, Park *et al*. 2009, Rota *et al*. 2010, Lagomarsino and Cattari 2013, Simões *et al*. 2015, Snoj and Dolšek 2017).

As an alternative to real records, simulated ground motions have been employed in response assessment of building structures previously (e.g., Atkinson and Goda 2010, Atkinson *et al*. 2011, Galasso *et al*. 2012, Karimzadeh *et al*. 2017a, 2017b, Karimzadeh 2019). There are some specific studies that have used simulated ground motion datasets for the derivation of fragility curves (e.g., Ellingwood *et al*. 2007, Karimzadeh *et al*. 2017d, Sisi *et al*. 2018).

As a novel contribution, the aim of this study is to compare fragility curves utilizing real and simulated ground motion records. Furthermore, the effects of ground motion variability and two different fragility curve derivation approaches on the whole set of derived fragility curves are investigated. As the final contribution, damage levels estimated for the fragility curves derived using alternative approaches are compared with the observed damage levels from the 1992 Erzincan (Turkey) earthquake (Mw=6.6) for verification purposes. For simulation of records that reflect regional seismic characteristics of the study area, the stochastic finite-fault simulation method as proposed by Motazedian and Atkinson (2005) is used. The validated regional input parameters are used for ground motion simulations of the scenario events (Karimzadeh *et al*. 2018). On the other hand, the real records are chosen from Pacific Earthquake Engineering Research Center's (PEER) global ground motion database including worldwide different earthquakes (Ancheta *et al*. 2013).

In this study, both real and simulated records are applied to a complete set of representative masonry buildings from Erzincan region using simplified structural models. The reason of selecting masonry buildings in this study for fragility analysis is that they constitute the significant part (approximately 60%) of the buildings in the study area (TUIK 2017) particularly in the shaded districts shown in

*Corresponding author, Ph.D.
E-mail: shaghkn@metu.edu.tr
[a]Ph.D.
[b]Professor

http://www.techno-press.org/?journal=eas&subpage=7 ISSN: 2092-7614 (Print), 2092-7622 (Online)

Fig. 1(a). The global building parameters of the regional construction practice are obtained by a walk-down survey conducted in the region of interest (Karimzadeh *et al*. 2017c, 2017d, 2018). Then, these parameters are used to idealize building models in the form of equivalent single-degree-of-freedom (ESDOF) systems for which nonlinear dynamic analyses are carried out using the real and simulated ground motion records. Next, simulated records-based and real records-based fragility curves are developed. Finally, damage estimation of a past earthquake in Erzincan is performed for the selected districts using the fragility curves and the results are compared with the observations.

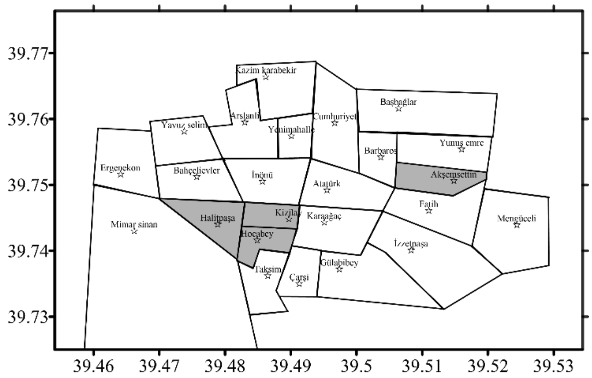

Fig. 1(a) The selected districts within Erzincan city center (dark grey polygon in part c) studied in this paper

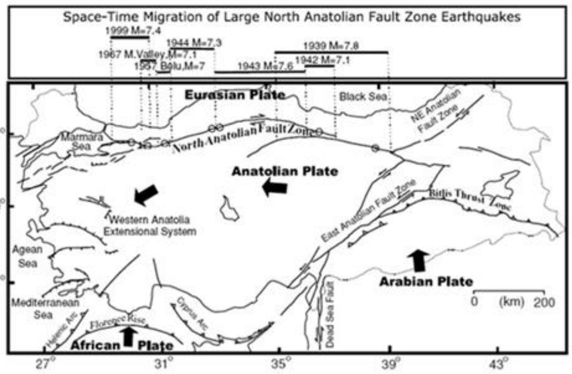

Fig. 1(b) Tectonic structure of the region and major seismic events on the North Anatolian Fault Zone in the last (adapted from Utkucu *et al*. 2003)

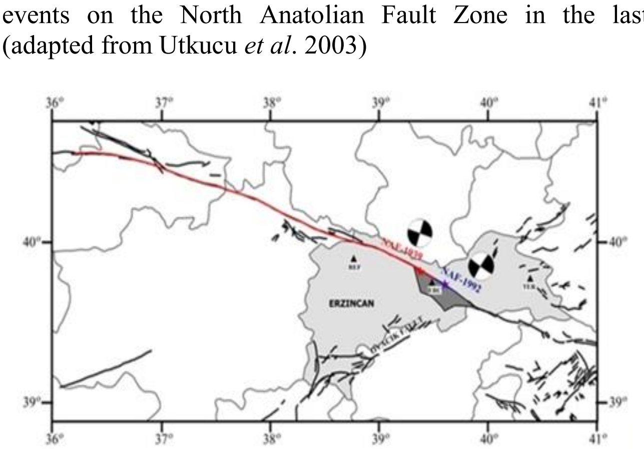

Fig. 1(c) Seismotectonics in the Erzincan region with the fa ult systems and the epicenters of the 1939 and 1992 events (adapted from Askan *et al*. 2013)

2. Study area

Erzincan is selected in this study, since it is set on active eastern segments of North Anatolian Fault Zone (NAFZ). In Northern Turkey, the active right-lateral strike-slip NAFZ caused many destructive earthquakes in history. The 1939 Erzincan (Eastern Turkey, Ms~8.0), 1992 Erzincan (Eastern Turkey, *Mw*=6.6), 1999 Kocaeli (Western Turkey, *Mw*=7.4) and 1999 Duzce (Western Turkey, *Mw*=7.2) earthquakes (Fig. 1(b)) could be given as examples of these destructive seismic events. There are many studies concentrating on the western part of NAFZ due to the existence of dense population and several critical industrial facilities. However, Erzincan area, resting on the eastern part of NAFZ, has not attracted enough attention despite its high seismicity. Therefore, it seems crucial to study this region as Erzincan is set on a deep alluvial basin and located at the tectonically complex conjunction point of three strike-slip faults: The left lateral North East Anatolian Fault, the right lateral North Anatolian Fault and the left lateral Ovacik fault (Fig. 1(c)). According to historical records (Askan *et al*. 2015), an approximate number of twenty severe earthquakes hit the Erzincan region in the last 1000 years. Despite this level of seismicity, the region has an inadequate number of seismic monitoring stations leading to limited ground motion records from real events. Additionally, majority of the existing unreinforced masonry building stock in this region is highly vulnerable. Due to these concerns, Erzincan is considered to be an ideal location for this study.

3. Simulated and real ground motion datasets

Seismic loss assessment in any region requires a suitable ground motion dataset compatible with the regional seismicity. Herein, for investigation of the consequence of seismic hazard in the fragility curves derived and corresponding estimated damage levels, two alternative ground motion datasets are considered: Simulated as well as real ground motion records. In order to set simulated ground motion records specific to the region of interest, simulations are performed for eastern part of North Anatolian Fault Zone. In this study, stochastic method (Boore 1983, 2003, 2009, Beresnev and Atkinson 1997, Motazedian and Atkinson 2005) is employed to generate simulated records, since it is preferred to simulate the frequency bound of engineering concern (e.g., Ugurhan and Askan 2010, Askan *et al*. 2015, Askan *et al*. 2017, Karimzadeh *et al*. 2017a, 2017b, 2017c, 2017d, Sokolov and Zahran 2018, Sun *et al*. 2018). For ground motion simulation, the stochastic finite-fault technique with dynamic corner frequency is used in this study (Motazedian and Atkinson 2005). EXSIM software is employed where the rupture plane is divided into fine sub-faults, each of which is considered as a point-source (Hartzell 1978). So as to generate the ground-shaking from the full rupture plane, the whole contribution resulting from an individual sub-fault is summed at an observation site considering appropriate time delays. The following formula presents the acceleration spectrum of the ij^{th} subfault

$$A_{ij}(f) = CM_{0ij}H_{ij}\left[(2\pi f)^2/\left[1 + \left(\frac{f}{f_{c_{ij}}}\right)^2\right]\right]e^{-\frac{\pi f R_{ij}}{Q(f)\beta}}G(R_{ij})A(f)e^{-\pi\kappa f} \tag{1}$$

where $C = \Re^{\theta\varphi} \cdot \sqrt{2}/4\pi\rho\beta^3$ and H_{ij} represent scaling factors, $\Re^{\theta\varphi}$ denotes radiation pattern, ρ is the density, β is the shear-wave velocity, $M_{0_{ij}} = M_0 S_{ij}/\sum_{k=1}^{nl}\sum_{l=1}^{nw} S_{kl}$ corresponds to the seismic moment, S_{ij} represents the relative slip weight and $f_{c_{ij}}(t) = N_R(t)^{-1/3}4.9 \times 10^6\beta(\Delta\sigma/M_{0_{ave}})^{1/3}$ denotes the ij^{th} sub-fault's dynamic corner frequency. The term $\Delta\sigma$ herein is the stress drop, $N_R(t)$ is the total number of sub-faults that ruptured at time t, and $M_{0_{ave}} = M_0/N$ is the seismic moment of sub-faults in average. R_{ij} is the distance of ij^{th} sub-fault from the site, $Q(f)$ denotes the quality factor, $G(R_{ij})$ represents the geometric spreading factor, $A(f)$ represents the site amplification, and $e^{-\pi\kappa f}$ stands for a high-cut filter (Anderson and Hough 1984). Further details can be found in Motazedian and Atkinson (2005).

Simulations are carried out for the 1992 Erzincan Earthquake (Turkey, *Mw*=6.6) and for different scenario events between 5.0 and 7.5 with an interval of 0.5. For simulation of each scenario event, a total of 123 nodes inside of a rectangular area (bordered by 39.70° to 39.78° latitudes and 39.45° to 39.54° longitudes) is considered. The spacing for grid points is approximately 1 km. Among the selected grid points, the nine of them are the locations with the available detailed soil profiles (Askan *et al*. 2015). It is known that local soil profile has an important effect in the ground motion amplitudes of the corresponding soil surface. At grid points without detailed soil information, Vs30 value at the closest station is assigned. The final error by this sort of assumptions is believed to be negligible since the distance in between the nodes is short enough. For ground motion simulation of the 1992 Erzincan event, all input parameters are taken from Askan *et al*. (2013) where validations were performed. In this study, these parameters are adapted and modified whenever necessary for different scenarios according to the magnitude of each event. Further information corresponding to ground motion simulation of the scenarios is given in Karimzadeh *et al*. (2018). It is noted that the Erzincan 1992 earthquake was recorded mostly at near-field stations. Thus, the simulations have also been validated at these stations where detailed simulation parameters (such as propagation and soil models) were available (Askan *et al*. 2015). Even though, there is a station located at 60 km from the source, there was not a detailed soil model there. As a result, in this study, the reliability of the simulations is valid at mostly near-field locations.

Next, to generate fragility curves, a database with 200 records having the highest PGA level of 1g is selected from the 861 time histories available from the simulated records database. These records are selected by checking the PGA values and making sure that there are 10 records per each PGA bin where ΔPGA=0.05 g. While selecting these records, it is aimed to obtain ground motion variability in terms of *Mw*, source-to-site distances and soil conditions. Thus, there are 20 bins and 10 records/bin which makes a total of 200 records in order to induce the entire range of structural response from no damage to collapse (Karimzadeh *et al*. 2018). The selected ground motion records cover a wide moment magnitude range (5.0-7.5) and source-to-site distances between 0.26 to 17.55 kilometers. Yet, the distance range of simulated data is not wide by global standards due to the reasons explained previously. It is noted that this can bring certain limitations to the findings.

Similar to the simulated records, the real records are selected to be compatible with the seismological features of the study area. The NGA-West2 database of PEER is utilized to select the real records with following characteristics; moment magnitude values between 5.0-7.5; strike-slip fault type, Joyner-Boore distance between 0-20 km and Vs30 between 220-500 m/s (Ancheta *et al*. 2013). For this purpose, initially, a total of 184 real records are selected. Among these 184 records, 113 of them are placed into the bins. However, since 113 records are not enough to cover the 10 records per each bin for 20 bins; another 87 records within the original 184 dataset are selected and linearly scaled to make a total of 200 real records with a PGA band of 0.05-1 g.

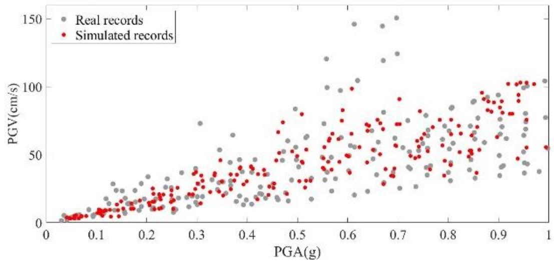

(a) PGV

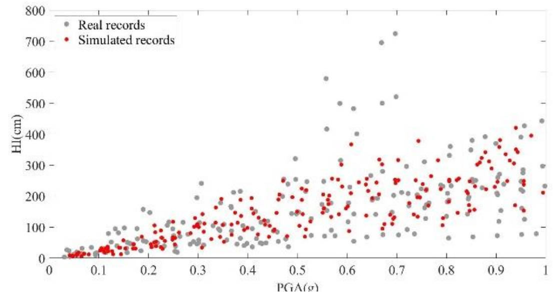

(b) HI

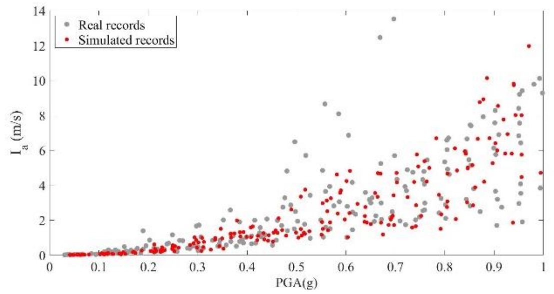

(c) I_a

Fig. 2 Variation of the real and simulated records in terms of the selected ground motion intensity parameters versus PGA where the grey and red dots correspond to the real and simulated records, respectively

Records from both datasets are filtered using baseline correction and 4th-order bandpass Butterworth filter type (between frequencies of 0.25 to 25 *Hz*). Next, peak ground acceleration, peak ground velocity (PGV), Arias intensity (I_a), and Housner Intensity (HI) are obtained for every ground motion record as comparatively shown in Fig. 2. The objective of this figure is to display the similarities and differences between the two alternative datasets used in the fragility analyses. The distribution reveals that regional variability is taken into account for each PGA level. Another observation is that simulated records are consistent with the real records in terms of the selected ground motion intensity parameters. This observation is also promising in terms of using simulated motions in earthquake engineering practice.

4. Description of masonry buildings

It is necessary to consider realistic buildings in any seismic loss estimation study. For masonry building classes, a broad range of seismic responses is observed as they are in general non-engineered buildings with structural deficiencies concerning the material quality as well as the construction practice (uneven arrangement of masonry walls, inadequate wall lengths, poor workmanship and maintenance, etc.). A walk-down survey is conducted resulting in a total of 9 subclasses for all masonry buildings in Erzincan (Karimzadeh *et al*. 2018). Two sample masonry structures from Erzincan are presented in Fig. 3. The survey assessment revealed that the masonry buildings under concern can be grouped according to some main structural parameters, such that the masonry buildings in the same sub-class show similar dynamic behavior under the same level of seismic intensity. For classification of the buildings, two major parameters considered are floor numbers and compliance level with respect to seismic design codes. The number of stories is considered to be 1-2-3 while the compliance levels are A (for high), B (for moderate) and C (for low). The abbreviated name for each subclass includes URM as unreinforced masonry, a digit showing the number of floors, and a letter showing the compliance level. For instance, URM2A corresponds to 2-story unreinforced masonry (URM) building class with the high compliance level. For estimation of the dynamic response of structures under severe earthquakes, performing elastic analyses, in general, is believed not to be adequately realistic for assessing the complexity of potential failure modes. In comparison, inelastic time history analysis is supposed to predict more accurate dynamic response. In this study, the dynamic structural response is assessed using the nonlinear time history analysis (NLTHA) of ESDOF systems performed on OpenSees software platform (http://opensees.berkeley.edu). The dynamic analyses are conducted using simplified models by idealizing detailed multi-degree-of-freedom (MDOF) models. These MDOF models were developed in a previous study (Erberik 2008) using MAS, a structural analysis program for masonry buildings (Mengi *et al*. 1992). The program is based on the nonlinear in-plane behavior of macro wall models. Nonlinear static analyses are conducted by the MAS to obtain the pushover curves (base shear force against the roof

(a) Two story masonry building

(b) One story masonry building

Fig. 3 Sample masonry buildings from Erzincan region

drift) of the models. Then, the generated curves are transformed into force versus displacement curves of ESDOF systems using the approach in FEMA 440 (ATC 2004). Finally, bilinearized parameters of these idealized ESDOF curves are determined for each subclass and these parameters are employed for NLTHA in OpenSees. In order to assess accurate dynamic responses of ESDOF models through NLTHA, it is necessary to consider a robust hysteresis model so that the inherent cyclic features of every building subclass subjected to ground shakings can be simulated. Among the various benchmark hysteresis models (Clough and Johnston 1966, Takeda *et al*. 1970) and more recent ones in the literature (Stojadinovic and Thewalt 1996, Sivaselvan and Reinhorn 1999, Sucuoglu and Erberik 2004, Park 2013, Graziotti *et al*. 2016), the Modified Ibarra-Medina-Krawinkler model with peak-oriented hysteretic response (Ibarra *et al*. 2005) is utilized for representing the ESDOF systems in this study. This hysteresis model has been proven to be suitable for different types of structures and components since it covers a wide range of parameters. This hysteresis model can also be used for masonry structures since it is able to simulate their limited ductility capacity as well as severe stiffness and strength degradation characteristics. Fig. 4 presents the backbone curve of this hysteresis model. In this figure, the term K_e is the elastic stiffness, F_y is the yield strength, α_s corresponds to the post-yield slope (α_s=K_s/K_e) where K_s is the pre-capping stiffness. Backbone curve degradation of this model starts with a softening branch at δ_c (as cap deformation) which represents the deformation corresponding to the peak strength in the force-deformation curve. The term μ is the ductility ratio defined as the ratio of the δ_c to δ_y (the yield deformation). The parameter α_c stands for the ratio of the post-capping

Table 1 Proposed ESDOF parameters for all URM building subclasses (The symbols are as explained within the text)

URM Subclass	*T (s)*		η		μ		α_s (%)	α_c (%)	λ
	Mean	Standard deviation	Mean	Standard deviation	Mean	Standard deviation			
URM1A			0.86	0.17	3.53	0.71	0	-20	0.20
URM1B	0.06	0.02	0.64	0.13	3.43	0.69	0	-25	0.20
URM1C			0.38	0.08	3.32	0.66	0	-30	0.20
URM2A			0.69	0.17	2.75	0.69	0	-20	0.20
URM2B	0.12	0.03	0.43	0.11	2.62	0.66	0	-25	0.20
URM2C			0.23	0.06	2.56	0.64	0	-30	0.20
URM3A			0.43	0.13	2.20	0.66	0	-20	0.20
URM3B	0.17	0.05	0.27	0.08	2.12	0.64	0	-25	0.20
URM3C			0.14	0.04	2.05	0.62	0	-30	0.20

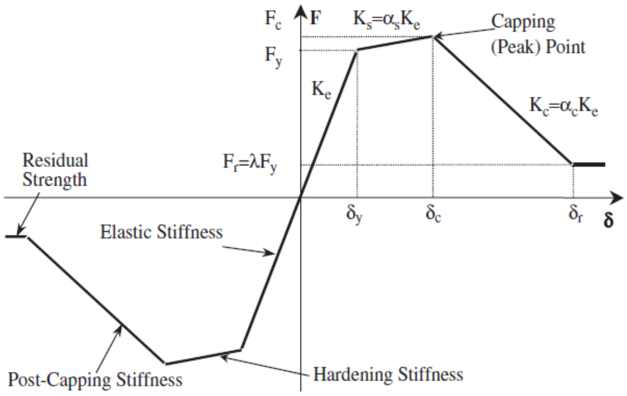

Fig. 4 Backbone curve for hysteresis model (adopted from Ibarra *et al*. 2005)

stiffness to K_e with mostly a negative value due to the descending branch (α_c=K_c/K_e). The term F_r presents the residual strength as a fraction of the yield strength (F_r=λF_y). In addition, δ_r stands for the deformation at the residual strength.

Equivalent SDOF parameters in terms of period (*T*), ductility factor (μ) and strength ratio (η) are determined as random variables for nine subclasses while the remaining parameters are assumed as constant. Table 1 summarizes the ESDOF parameters defined for all building subclasses (Karimzadeh *et al*. 2017c, 2017d, 2018). Both random and constant parameters were initially obtained in a national research project regarding Erzincan city, by examining a vast number of references about global structural characteristics of Turkish masonry buildings (Karimzadeh *et al*. 2018). In this work, Latin hypercube sampling method is applied to simulate 20 samples for each URM subclass. For this purpose, period, ductility ratio and strength factor are considered as random variables by the assumption of lognormal distribution (Olsson *et al*. 2003).

5. Fragility analyses

In order to derive fragility curves, ESDOF time history analyses are conducted for the real and simulated record sets as discussed in Section 3. To accomplish this purpose, LS1-Immediate Occupancy, LS2-Life Safety and LS3-Collapse Prevention are taken as the performance levels. Fragility curves are derived based on the limit states defined previously by Karimzadeh *et al*. (2018) for the performance levels. In that study, the limit states were determined by examining two previous studies with detailed information on the seismic behavior of masonry buildings (Calvi 1999, Erberik 2008). Accordingly, drift limits have been proposed for these three performance levels as 0.03%, 0.1% and 0.5%, respectively and these values are converted into spectral displacement limits of ESDOF systems by making use of the assigned structural parameters and floor number of each building subclass.

In the first stage of the study, for investigation of the effect of seismic hazard in the derivation of final fragility curves two alternative record sets including simulated and real ground motion time histories are considered. As the next step, two sub-groups with different set size of ground motion records are considered for both real and simulated record sets to evaluate the effect of variability in ground motion on fragility results. In the final step, the sensitivity of fragility curve calculation methods is performed considering alternative probability distribution functions.

5.1 Evaluation of the effect of employing different ground motion datasets

In this section, the effect of employing alternative ground motion time histories is investigated using simulated and real sets and the effect of variability in seismic demand is further evaluated by considering alternative sub-groups with different ground motion dataset size. For both real and simulated datasets, alternative sub-groups including 200- and 20-records are formed. The first sub-group (200 records) is selected to introduce ground motion variability in seismic demand, while the second sub-group (10 alternative sets with 20 records) neglects this variability. In the formation of 200-record sub-group, 10 records at each intensity level are employed. On the other hand, in the formation of 20-record sub-group alternatives, 1 record from each PGA bin is randomly selected in order to eliminate the ground motion variability in the PGA bin.

5.2 Evaluation of the effect of different fragility curve determination methods

Starting with the early work of Shinozuka *et al*. (2000), there are recent studies about the efficiency of different fragility curve generation approaches (Celik and Ellingwood 2010, Baker 2015, Lallemant *et al.* 2015). These studies have comparatively evaluated the alternative approaches for derivation of fragility curves. As an extension, in this study, to examine the sensitivity of the fragility curves to the derivation techniques, two alternative approaches are applied. The assumption of the normal distribution function is useful when the size of sample points is large enough and the scatter dataset fits the normal distribution. Frequency analysis, instead, which is based on a direct counting of the dataset above each limit state is always accurate when the analysis is performed with a sufficient and complete set of sample points. The advantage of frequency analysis is that distribution of data points is not considered whereas in the case of normal fit an assumption is made.

Fig. 5 displays the two alternative approaches considered in this study. In the first phase, all values of the maximum ESDOF displacements are plotted for discrete intervals of the selected ground motion intensity parameter (PGA) (Fig. 5(a)). The target limit state (LS_i) for the maximum ESDOF displacement is represented by the horizontal line on the vertical axis. The only difference between the two approaches appears in the second phase: The first one is based on a normal distribution assumption for the responses at each intensity level (Fig. 5(b).1). In other words, a normal distribution is applied to signify the scatter plot of maximum ESDOF displacements at a given intensity. This method is named as the ND-based method since it uses Normal Distribution for the response. In contrast, the second method, named as FA-based, employs Frequency Analysis by calculating the ratio of the overall number of responses above a specified limit state to the total number of responses computed at a specific intensity level (Fig. 5(b).2). Equations 2 and 3 show the mathematical formulation of ND-based and FA-based determination methods, respectively

$$P[D \geq LS_i|GMI_j] = a_A \tag{2}$$

$$P[D \geq LS_i|GMI_j] = \frac{n_A}{n_T} \tag{3}$$

where a_A in Equation 2 stands for the entire area above the limit state i (LS_i). The terms n_A and n_T in Equation 3 are the total number of responses equal or larger than the i^{th} limit state, and the total number of responses, respectively, at the intensity level j (GMI_j). The fragility curves are obtained by plotting the exceedance probability of a limit state at a specific ground motion intensity. A complete plot of discrete values for the probability of exceedance (PoE) at the selected limit state versus PGA is obtained (Fig. 5(c)). Finally, the fragility curve is generated by fitting a cumulative lognormal probability distribution function to these discrete values based on least squares approach (Fig. 5(d)).

These steps are repeated for all URM building subclasses at all levels of PGA to obtain fragilities for the selected previously defined limit states employed.

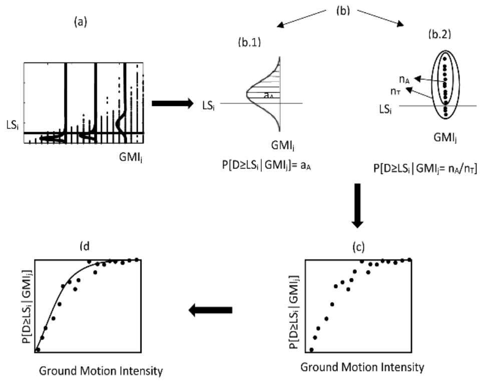

Fig. 5 Schematic representation of the alternative fragility curve generation procedures

5.3 Discussion on the developed fragility curves

In this part, results corresponding to the generated fragility curves from alternative approaches using either different ground motion set or fragility curve generation procedures are presented. Fig. 6 compares the ND-method based fragility curves using the 200-record subgroups for both Simulated (S) and Real (R) ground motions. Due to the space reasons, the results are only presented for the three selected building subclasses with different performance levels. Examination of Fig. 6 reveals that the difference between simulated- and real-record-based results is not so significant. For all subclasses and limit states except LS3, simulated records provide slightly higher Damage State (DS) probabilities at all ground motion intensities compared to those of real records. For LS3 and especially for 3-story URM models, median values of the simulated-record-based fragility curves are higher whereas dispersion values are less, which causes lower probabilities at low PGA levels and higher probabilities at high PGA levels when compared to the real-record-based fragility curves. In general, all other cases indicate similar results.

Fig. 7 comparatively shows the results of FA-method based fragilities for simulated and real ground motion records employing 200-record subgroup. Due to the space reasons, the results are given for three other building subclasses. In general, comparison of FA-method based fragility curves reveals that for all subclasses at three limit states, simulated record dataset results in slightly larger values of probability of exceedance than those of real records. Comparison of the fragility results for Immediate Occupancy limit state as presented in Figs. 6 and 7 yields insignificant difference for all subclasses. For the other limit states including Life Safety and Collapse Prevention, in contrast, there is a noticeable difference which is more pronounced for high ground motion intensity levels. Maximum differences in terms of exceedance probabilities in Figs. 6 and 7 considering all subclasses reach up to 0.17 and 0.10, respectively. The overall examination of the entire (i.e., both ND-based and FA-based) fragility results employing 200-record simulated and real datasets yields a broad range of seismic responses consistent with the structural characteristics of all subclasses considered. In

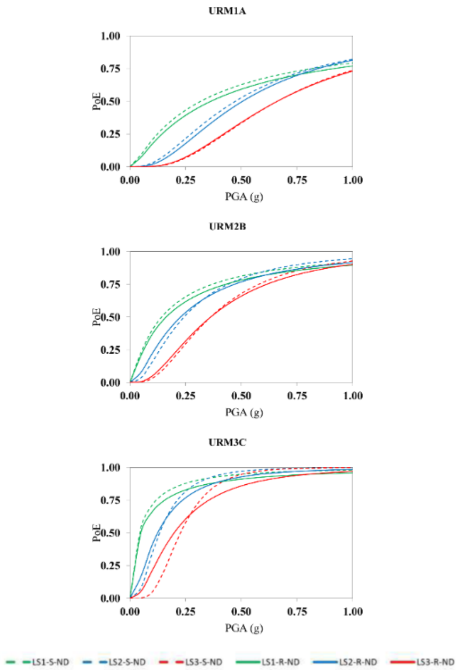

Fig. 6 ND-method based fragility results for both simulated and real 200-record datasets

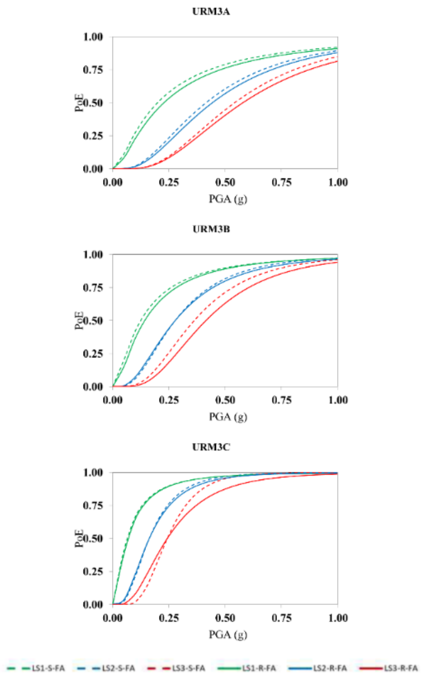

Fig. 7 FA-method based fragility results for both simulated and real 200-record datasets

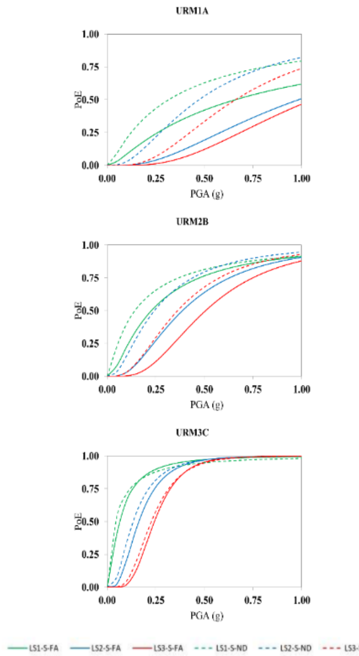

Fig. 8 Comparison of FA-based and ND-based fragility results using simulated 200-record dataset

other words, it is observed that URM buildings become more vulnerable as the number of floors increases and the code compliance level becomes lower regardless of the generation technique or ground motion features. The increase in seismic vulnerability with number of floors is mostly due to the fact that URM buildings in the region of interest are non-standard structures with lack of an engineering supervision resulting in a poor quality of materials and construction. This is actually an expected trend which is stated in previous studies including Erberik (2008), Cattari *et al.* (2014) and Derakhshan and Griffith (2018).

If the curves for the selected three subclasses of Fig. 6 are compared for the two alternative methods using 200 simulated record set, ND-based method fragilities are observed to be greater than FA-based method curves (Fig. 8). The difference becomes significant for high quality and one-story masonry classes (e.g., URM1A). As the number of floors increases and the code compliance level decreases, the difference becomes less (e.g., URM3C). The maximum difference among fragilities of all subclasses is approximately 0.35 (in terms of PoE) observed for subclasses URM1A and URM1C. The large difference between the two methods observed for URM1A in Fig. 8 is due to relatively poor representation of the data at certain ranges by normal distribution. On the other hand, there is a smaller difference between the two methods for URM2B and URM3C since majority of the data for these classes follow normal distribution. The comparisons of fragility curves obtained from different approaches indicate that different methods employed here (in this study ND-based and FA-based approaches) can affect the fragility results. Therefore, it seems critical to compare and validate the efficiency of alternative fragility curve determination approaches.

Fig. 9 presents the FA-based fragility curves developed based on simulated records for the three selected subclasses with moderate compliance level. In this figure, the effect of ground motion variability is investigated. Since the real and simulated datasets are compatible with each other, the differences in the fragility curves due to ground motion variability is small. The results reveal that the fragilities from 200-record subgroup stay almost within ±1standard deviation (i.e., sigma) of the mean of the curves obtained

Table 2 Information corresponding to the selected districts in Erzincan region

Name of District	Latitude (°)	Longitude (°)	Site Class (NEHRP)	Simulated PGA (g)	Masonry w.r.t. Total Stock (%)	1-Story URM (%)	2-Story URM (%)	3-Story URM (%)
Kizilay	39.7448	39.4897	C	0.6406	90	95	2	3
Aksemsettin	39.7506	39.5148	C	0.6374	90	90	8	2
Halitpasa	39.7440	39.4789	C	0.3698	94	65	25	10
Hocabey	39.7416	39.4849	C	0.4191	96	74	19	7

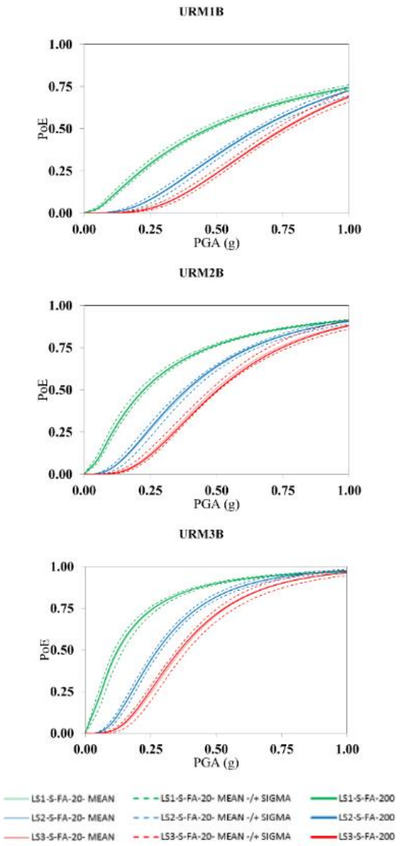

Fig. 9 Comparison of FA-based fragility results for simulated 200- and 20-record datasets

from 20-record subgroup alternatives. The observed variation between the results, although not very significant, obtained from 20-record group shows the influence of variability in ground motion (in terms of magnitude, site characteristics and distance from source-to-site) for a specific intensity level in the fragility results. Note that 20-record groups are extracted from the 200-record group set, which might be the reason for insignificant variation between the mean values. In addition, if the curves are expressed for more than 1 standard deviation, the difference among the 20-record set results becomes more significant.

6. Comparison of the generated fragility curves using seismic damage estimation for the 1992 Erzincan (Turkey, *Mw*=6.6) event

This section aims to compare the generated fragilitycurves for URM structures with the observed damage. For this purpose, seismic damage is estimated for the 1992 Erzincan (Turkey, *Mw*=6.6) earthquake using fragility curves presented previously. In order to investigate the influence of alternative datasets and approaches for fragility computations, estimated damage values are compared with the damage values observed during the 1992 (*Mw*=6.6) Erzincan event. In this study, since the fragility curves are obtained for masonry buildings, only the districts with the higher density of masonry buildings (greater than 90% of total building types) are considered. For this purpose, four residential districts are chosen in the region of interest. The fundamental steps to estimate seismic damage in the selected districts are as follows:

- Simulated records of the 1992 Erzincan earthquake within the selected districts are compiled.
- Since fragility curves for masonry buildings are generated with PGA as the ground motion intensity parameter, simulated PGAs are obtained at the center of all districts.
- Percent distribution of the URM structures regarding the story numbers and compliance level for the selected districts is determined.
- Damage Probability Matrices (DPMs) for the masonry structural types in the districts for the corresponding PGA values are constructed. DPMs are formed following the original approach by Whitman (1973).
- Lastly, for each district at its center, a single Mean Damage Ratio (MDR) is obtained. MDR uses a single value to express the disaggregated damage estimates (as implemented by Askan and Yucemen 2010). MDR is commonly used for comparison and validation of fragility curves because the observed damage data collected in the field surveys can be practically expressed in terms of MDR.

Table 2 gives the latitudes, longitudes, simulated PGA values, distribution of the masonry buildings with respect to the story numbers and the code compliance in the selected districts. It is observed that the Kizilay and Aksemsettin districts located at closer distances from the fault plane naturally experience higher PGA values than Halitpasa and Hocabey districts which are located at larger distances from the fault plane. Structure-specific information is gathered from the walk-down survey conducted in Erzincan (Karimzadeh *et al*. 2018). In order to compute MDRs at the selected residential districts, firstly DPMs are formed. Each row of DPM corresponds to a certain seismic damage state while each column of the matrix corresponds to a constant seismic intensity level. Finally, each element, denoted by P_k (DS, I), stands for the PoE at a specified DS and seismic intensity level of I. The definition is simply expressed as follows

$$P_k(DS, I) = \frac{N(DS, I)}{N(I)} \quad (4)$$

where $N(I)$ represents the number of k^{th}-type of structures subjected to seismic intensity level of I, while N (DS, I) corresponds to the total number of buildings at (DS) damage state among $N(I)$.

The damage probability matrix given by Gurpinar *et al.* (1978) for Turkey considers 5 different groups for damage states: N: No damage, L: Light damage, M: Moderate damage, H: Heavy damage, and C: Collapse. The level of damage (either structural or non-structural) for each intensity level and building type is represented by each damage state. Damage Ratio (DR) represents the physical damage state of the building quantitatively, so a range of DR is typically specified for each damage state. DR corresponding to each damage state is determined using Table 3 given in Gurpinar *et al.* (1978). In Table 3, DRs and Central Damage Ratios (CDRs) are given for five damage states. The CDR indicates a unique value corresponding to each damage state. In this study, only four damage states are used; using the first three and combining the last two given in Table 3. It is noted that these CDR values are consistent with the current global values (ATC 13). The study of Askan and Yucemen (2010) showed that these DR and CDR values are still valid for buildings in Turkey since the verification in that study is based on the damage data from the 1999 Marmara earthquakes.

In this study, since 3 limit states (LS1, LS2, LS3) are considered for derivation of fragility curves for a single building class, a total of 4 damage states is considered as DS_1 for none, DS_2 for light, DS_3 for moderate and DS_4 for severe. It is noted that for the damage states defined in this study except severe DS, the statistical values provided by Gurpinar *et al.* (1978) are considered. The CDR for DS_4 is taken as the mean of two central damage ratios (H and C) by Gurpinar *et al.* (1978) that is 85%.

Table 3 Verbal descriptions, damage ratios and central damage ratios corresponding to each damage state (Whitman 1973, Gurpinar *et al.* 1978)

Damage State	Verbal Description	Damage Ratios (%)	Central Damage Ratio (%)
No Damage	No Damage	0-1	0
Light Damage	Minor structural damage, obvious cracking or yielding in a few structural members; substantial non-structural damage with widespread cracking	1-10	5
Moderate Damage	Substantial structural damage requiring repair or replacement of any structural members; associated non-structural damage requiring repairs to major portion of interior; building vacated during repairs	10-50	30
Heavy Damage	Condemned building	50-90	70
Collapse	Collapsed building	90-100	100

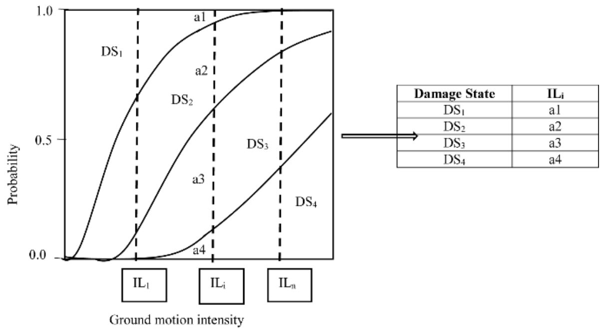

Fig. 10 Construction of a DPM from a set of fragility curves

In this study, DPMs for the selected districts are formed using the information provided by alternative fragility curves (Figs. 6 and 7). Fig. 10 shows the steps of deriving a DPM from an existing fragility curve for 4 different damage states (DS_1, DS_2, DS_3 and DS_4) at ground motion intensity level of i (IL_i). In order to calculate the damage probabilities at different states corresponding to a certain ground motion intensity level (IL_i), a vertical line is intersected to the fragility curve at that intensity level. Then, the portions between any two limit states are calculated to obtain the damage state probabilities. For each residential district, IL_i corresponds to the simulated PGA at the corresponding district center from the stochastic finite-fault methodology. Finally, in order to compute the MDRs at the selected residential districts, the following formula is used.

$$MDR(IL) = \sum_{DS} P_k(DS, IL).CDR(DS) \quad (5)$$

where, CDR(DS) is the central damage ratio at damage state DS, IL stands for the ground motion intensity level which is PGA of a certain residential district in this study.

For estimation of MDRs at the selected residential districts with dense number of URM building types, the results of four different approaches are used. Due to the importance of considering ground motion variability in the generated fragility curves, the fragility curves based on records with 200 records are considered only. Therefore, it is aimed herein to investigate the effect of using either real or simulated records along with two alternative fragility curve generation methods for damage estimation. Table 4 lists details corresponding to different approaches. In this study, the observed MDRs for the 1992 Erzincan earthquake are taken from the previous field studies by Sucuoglu and Tokyay (1992), Sengezer (1993), Erdik *et al.* (1994). Table 5 presents the damage levels observed during the 1992 Erzincan event along with the estimated MDRs from the abovementioned four different approaches. The results reveal that for Halitpasa and Hocabey districts, the estimated MDR values are less than those in Kizilay and Aksemsettin districts due to the lower PGA values at the first two locations. Overall, comparison of the observed versus predicted MDRs for the 1992 Erzincan event reveals that the accuracy of the second and fourth approaches (using FA-based fragilities) is higher than the accuracy of the first and third approaches (using NA-based fragilities). These differences may be attributed to both numerical and

Table 4 Ground motion dataset versus fragility information used in estimation of MDRs

ID	Ground Motion Records Set	Fragility Curve Generation Method
Approach 1: $MDR_{S\text{-}ND\text{-}200}$	Simulated 200-record-set	ND-based
Approach 2: $MDR_{S\text{-}FA\text{-}200}$	Simulated 200-record-set	FA-based
Approach 3: $MDR_{R\text{-}ND\text{-}200}$	Real 200-record-set	ND-based
Approach 4: $MDR_{R\text{-}FA\text{-}200}$	Real 200-record-set	FA-based

Table 5 Observed and predicted MDR values for the 1992 Erzincan event

District	Observed MDR (%)	Predicted MDR (%)			
		$MDR_{S\text{-}ND\text{-}200}$	$MDR_{S\text{-}FA\text{-}200}$	$MDR_{R\text{-}ND\text{-}200}$	$MDR_{R\text{-}FA\text{-}200}$
Kizilay	29.65	52.57	30.43	51.82	29.15
Aksemsettin	39.00	58.68	38.59	57.85	38.07
Halitpasa	13.54	33.60	16.22	33.29	14.60
Hocabey	13.83	37.32	18.31	36.72	16.71

Table 6 RMSE and coefficient of correlation for four different damage prediction approaches

Approach for Prediction of MDR	Error (RMSE)	Coefficient of Correlation
$MDR_{S\text{-}ND\text{-}200}$	21.6017	0.9883
$MDR_{S\text{-}FA\text{-}200}$	2.6471	0.9974
$MDR_{R\text{-}ND\text{-}200}$	20.9824	0.9892
$MDR_{R\text{-}FA\text{-}200}$	1.6202	0.9972

modeling uncertainties. A major source of uncertainty may arise from the fact that there are other types of buildings in the region even though the majority is masonry as assumed herein. In addition, the subjectivity in the assignment of damage levels for the buildings of each district in the field results in uncertainty. Results presented in Table 5 also reveal that both real and simulated records provide the same levels of MDRs in the selected districts while using the same fragility generation technique (either FA-based or ND-based).

Finally, for evaluation of the goodness of fit between the predicted damage values from different approaches and the observed damage levels, the Root Mean Square Error (RMSE) function is expressed as follows

$$RMSE = (\frac{1}{N}\sum_{i=1}^{N}(MDR(est)_i - MDR(obs)_i)^2)^{1/2} \qquad (6)$$

where N represents the number of the selected districts, which is 4 herein, $MDR(est)_i$ is the estimated MDR and $MDR(obs)_i$ is the observed MDR at i^{th} district. In addition, the correlation coefficients between the predicted (with four alternative techniques) and the observed MDRs are measured. The correlation coefficients and the relating RMSE values are listed in Table 6.

The comparison demonstrates that among the four approaches considered, the MDRs predicted using the second and fourth approaches ($MDR_{S\text{-}FA\text{-}200}$ and $MDR_{R\text{-}FA\text{-}200}$) have the highest correlation with the observed MDR levels where the correlation coefficients are 0.9974 and 0.9972, respectively. For these two approaches with FA-based fragilities, the RMSEs are less than the ones obtained in the approaches where normal distribution function is employed for generation of the fragility curves. Therefore, for the cases covered here, the assumption of frequency analysis for calculation of probabilities of exceedance in fragility curve generation methodology (Fig. 5(b).2) yields a more accurate estimation of observed damage levels due to better prediction of observed damage. The results also reveal that fragility curves obtained based on regionally simulated ground motions using stochastic finite-fault methodology yield reliable damage levels.

7. Conclusions

The fundamental motivation of the current work is to investigate the effect of alternative ground motion datasets and different fragility development approaches on the fragility curves. The proposed study is performed on masonry buildings in Erzincan (Eastern Turkey). The ground motion effects are studied in twofold: The first exercise involves derivation of fragility curves with both real versus simulated ground motion records compatible with the regional seismicity. The second one is concerned with effects of ground motion variability (20 versus 200 samples) on the derived fragility curves. As a result, effects of both fragility derivation approach and selected ground motion datasets are assessed in detail.

The comparison of resulting fragility curves is performed in terms of seismic damage levels for the 1992 Erzincan (Turkey) event. The mean damage ratios are estimated at selected districts with large number of masonry buildings. The estimated damage levels from alternative approaches are compared against the observed values during the 1992 Erzincan (Turkey) earthquake.

The findings of this study are naturally dependent on the assumptions and numerical approaches used in the analyses. In other words, the SDOF assumption along with its model parameters as well as the fragility derivation approaches used herein influence the main findings. Based on the models and assumptions presented in this study, the following conclusions are obtained:

• Comparison of the results from simulated versus real ground motions reveals that regardless of the fragility curve generation technique, the simulated ground motions generally yield slightly larger probability of exceedance with lower dispersion values compared to those of real records. This observation indicates that simulated ground motions could be used for generating region-specific fragility functions. This could be particularly necessary in regions with sparse near-field data from large earthquakes and regions of unevenly distributed seismic networks. Correspondingly, reliable fragility curves are derived if ground motion variability is included in simulated data (in terms of magnitude, source-to-site distances and soil conditions).

• Sensitivity analyses reveal that there is a significant difference between FA-based and ND-based fragility curves particularly for high-code single-story masonry classes. The effect of using either one of these techniques becomes insignificant for weak masonry classes with 3 stories.

• When ground motion variability is considered in sensitivity analyses (200- versus 20-record ground motion sets), it is observed that the results from larger ground motion set lie within one standard deviation of the mean curves obtained for the smaller datasets. The variation observed for different ground motion sets (including 20- and 200-record sets) demonstrates that the seismic hazard variability has a major influence on the obtained results. Thus, in development of fragility curves, it may become suitable to take into account the input motion variability considering magnitude, soil profile and distance from source-to-site for a specific ground motion intensity bin.

• Damage assessment of the 1992 Erzincan (Turkey) earthquake reveals that for both ground motion datasets (real and simulated records), the reliability of FA-based fragility curves is higher than the ND-based ones for the cases covered in this study. This observation indicates the importance of selecting the most suitable fragility generation method for more realistic damage estimation.

• Finally, comparison of the predicted damage values for the 1992 Erzincan event shows that while using the same fragility curve generation technique (either ND-based or FA-based), the difference between estimated damage levels from the real and simulated records is negligible. This observation indicates that use of simulated input motions is promising for seismic damage estimation studies in regions with sparse data or poor seismic networks.

This approach can be further extended to other seismically active areas in future as long as a validated synthetic (simulated) ground motion dataset is available in addition to a reliable local building inventory. The effect of alternative ground motion simulation techniques (such as deterministic and hybrid methods) on seismic damage estimation should also be investigated.

Acknowledgments

The data in this study has been collected with the financial support by a Turkish National Geodesy and Geophysics Union through the project with grant number TUJJB-UDP-01-12. The first author is partially funded by JICA-SATREPS through the MarDiM project entitled "Earthquake and Tsunami Disaster Mitigation in the Marmara Region and Disaster Education in Turkey". The second author has been financially supported by The Scientific and Technological Research Council of Turkey (TUBITAK) through Domestic Doctoral Scholarship Program. All these supports are highly acknowledged.

References

Ancheta, T.D., Darragh, R.B., Stewart, J.P., Seyhan, E., Silva, W.J., Chiou, B.S.J., Wooddell, K.E., Graves, R.W., Kottke, A.R., Boore, D.M., Kishida, T. and Donahue, J.L. (2013), "PEER NGA-West2 Database", PEER 2013/03, Pacific Earthquake Engineering Research Center.

Anderson, J. and Hough, S. (1984), "A model for the shape of the Fourier amplitude spectrum of acceleration at high frequencies", *Bull. Seismol. Soc. Am.*, **74**(5), 1969-1993.

Ansal, A., Akinci, A., Cultrera, G., Erdik, M., Pessina, V., Tonuk, G. and Ameri, G. (2009), "Loss estimation in Istanbul based on deterministic earthquake scenarios of the Marmara Sea region (Turkey)", *Soil Dyn. Earthq. Eng.*, **29**(4), 699-709. https://doi.org/10.1016/j.soildyn.2008.07.006.

Applied Technology Council, ATC (1985), Earthquake Damage Evaluation Data for California, ATC-13 Report, California, U.S.A.

Applied Technology Council, ATC (2004), FEMA 440, Improvement of Nonlinear Static Seismic Analysis Procedures, ATC-55 Project Report, prepared for the Federal Emergency Management Agency, Washington D.C., U.S.A.

Askan, A. and Yucemen, M.S. (2010), "Probabilistic methods for the estimation of potential seismic damage: Application to reinforced concrete buildings in Turkey", *Struct. Saf.*, **32**(4), 262-271. https://doi.org/10.1016/j.strusafe.2010.04.001.

Askan, A., Karimzadeh, S. and Bilal, M. (2017), "Seismic Intensity Maps for North Anatolian Fault Zone (Turkey) based on recorded and simulated ground motion data", Active Global Seismology, Neotectonics and Earthquake Potential of the Eastern Mediterranean Region, John Wiley and Sons, Inc., N.J, U.S.A.

Askan, A., Karimzadeh, S., Asten, M., Kilic, N., Sisman, F.N. and Erkmen, C. (2015), "Assessment of seismic hazard in Erzincan (Turkey) region: construction of local velocity models and evaluation of potential ground motions", *Turkish J. Earth. Sci.*, **24**(6), 529-565.

Askan, A., Sisman, F.N. and Ugurhan, B. (2013), "Stochastic strong ground motion simulations in sparsely-monitored regions: A validation and sensitivity study on the 13 March 1992 Erzincan (Turkey) earthquake", *Soil Dyn. Earthq. Eng.*, **55**, 170-181. https://doi.org/10.1016/j.soildyn.2013.09.014.

Atkinson, G.M. and Goda, K. (2010), "Inelastic seismic demand of observed versus simulated ground-motion records for Cascadia subduction earthquakes", *Bull. Seismol. Soc. Am.*, **100**(1), 102-115. https://doi.org/10.1785/0120090023.

Atkinson, G.M., Goda, K. and Assatourians, K. (2011), "Comparison of nonlinear structural responses for accelerograms simulated from the stochastic finite-fault approach versus the hybrid broadband approach", *Bull. Seismol. Soc. Am.*, **101**(6), 2967-2980. https://doi.org/10.1785/0120100308.

Baker, J.W. (2015), "Efficient analytical fragility function fitting using dynamic structural analysis", *Earthq. Spectra*, **31**(1), 579-599. https://doi.org/10.1193%2F021113EQS025M.

Beresnev, I. and Atkinson, G. (1997), "Modeling finite-fault radiation from the w^n spectrum", *Bull. Seismol. Soc. Am.*, **87**(1), 67-84.

Boore, D.M. (1983), "Stochastic simulation of high-frequency ground motions based on seismological models of the radiated spectra", *Bull. Seismol. Soc. Am.*, **73**(6), 1865-1894.

Boore, D.M. (2003), "Simulation of ground motion using the stochastic method", *Pure Appl. Geophys.*, **160**(3), 635-676. https://doi.org/10.1007/PL00012553.

Boore, D.M. (2009), "Comparing stochastic point-source and finite-source ground-motion simulations: SMSIM and EXSIM", *Bull. Seismol. Soc. Am.*, **99**(6), 3202-3216. https://doi.org/10.1785/0120090056.

Calvi, G.M. (1999), "A displacement-based approach for vulnerability evaluation of classes of buildings", *J. Earthq. Eng.*, **3**(3), 411-438.

Cattari, S., Lagomarsino S. and Ottonelli, D. (2014), "Fragility curves for masonry buildings from empirical and analytical models", *Proceedings of the 2nd Conference on Earthquake Engineering and Seismology*, Istanbul, Turkey, August.

Celik, O.C. and Ellingwood, B. (2010), "Seismic fragilities for non-ductile reinforced concrete frames-role of aleatoric and epistemic uncertainties", *Struct. Saf.*, **32**(1), 1-12. https://doi.org/10.1016/j.strusafe.2009.04.003.

Clough, R.W. and Johnston, S.B. (1966), "Effect of stiffness degradation on earthquake ductility requirements", *Proceedings of Japan Earthquake Engineering Symposium*, Japan.

Derakhshan, H. and Griffith, M.C. (2018). "Final report on fragility curves for URM building risk assessment in Australia", Bushfire and Natural Hazards Cooperative Research Centre, Melbourne, Australia.

Ellingwood, B., Celik, O.C. and Kinali, K. (2007), "Fragility assessment of building structural systems in mid-America", *Earthq. Eng. Struct. Dyn.*, **36**, 1935-1952. https://doi.org/10.1002/eqe.693.

Erberik, M.A. (2008), "Generation of fragility curves for Turkish masonry buildings considering in-plane failure modes", *Earthq. Eng. Struct. Dyn.*, **37**(3), 387-405. https://doi.org/10.1002/eqe.760.

Erdik, M., Yuzugullu, O., Karakoc, C., Yilmaz, C. and Akkas, N. (1994), "March 13, 1992 Erzincan (Turkey) earthquake", *Proceedings of the 10th World Conference on Earthquake Engineering*, Balkema, Rotterdam.

Galasso, C., Zareian, F., Iervolino, I. and Graves, R.W. (2012), "Elastic and post-elastic response of structures to hybrid broadband synthetic ground motions", *Proceedings of the 9th International Conference on Urban Earthquake Engineering and the 4th Asia Conference on Earthquake Engineering*, Tokyo Institute of Technology, Tokyo, Japan.

Gokkaya, K. (2016), "Geographic analysis of earthquake damage in Turkey between 1900 and 2012", *Geomat. Nat. Haz. Risk.*, **7**(6), 1948-1961. https://doi.org/10.1080/19475705.2016.1171259.

Graziotti, F., Penna, A. and Magenes, G. (2016). "A nonlinear SDOF model for the simplified evaluation of the displacement demand of low-rise URM buildings", *B. Earthq. Eng.*, **14**(6), 1589-1612. https://doi.org/10.1007/s10518-016-9896-5.

Gurpinar, A., Abali, M., Yucemen, M. and Yesilcay, Y. (1978), "Feasibility of obligatory earthquake insurance in Earthquake Engineering Research Center", Report 78-05, Civil Eng. Depart., Middle East Technical University, Turkey.

Hartzell, S. (1978), "Earthquake aftershocks as Green's functions", *Geophys. Res. Lett.*, **5**(1), 1-4. https://doi.org/10.1029/GL005i001p00001.

Ibarra, L.F., Medina, R.A. and Krawinkler, H. (2005), "Hysteretic models that incorporate strength and stiffness deterioration", *Earthq. Eng. Struc. Dyn.*, **34**(12), 1489-511. https://doi.org/10.1002/eqe.495.

Karimzadeh, S. (2019). "Seismological and engineering demand misfits for evaluating simulated ground motion records", *Appl. Sci.*, **9**(21), 4497. https://doi.org/10.3390/app9214497.

Karimzadeh, S., Askan, A. and Yakut, A. (2017b), "Assessment of simulated ground motions for their use in structural engineering practice; a case study for Duzce (Turkey)", *Pure Appl. Geophys.*, **174**(9), 3325-3329.

Karimzadeh, S., Askan, A., Erberik, M.A. and Yakut A. (2018). "Seismic damage assessment based on regional synthetic ground motion dataset: a case study for Erzincan, Turkey", *Nat. Hazard.*, **92**(3), 1-25. https://doi.org/10.1007/s11069-018-3255-6.

Karimzadeh, S., Askan, A., Erberik, M.A. and Yakut, A. (2017c), "Seismic damage assessment in Erzincan (Turkey) utilizing synthetic ground motion records", *Proceedings of the 16th World Conference on Earthquake Engineering*, Santiago, Chile.

Karimzadeh, S., Askan, A., Yakut, A. and Ameri, G. (2017a), "Assessment of alternative simulation techniques in nonlinear time history analyses of multi-story frame buildings: A case study", *Soil Dyn. Earthq. Eng.*, **98**, 38-53. https://doi.org/10.1016/j.soildyn.2017.04.004.

Karimzadeh, S., Kadas, K., Erberik, M.A., Askan, A. and Yakut, A. (2017d), "A Study on fragility analyses of masonry buildings in erzincan (Turkey) utilizing simulated and real ground motion records", *Proceedings of the 10th International Conference on Structural Dynamics (EURODYN)*, Rome, Italy.

Lagomarsino, S. and Cattari, S. (2013), "Fragility functions of masonry buildings", SYNER-G: Typology Definition and Fragility Functions for Physical Elements at Seismic Risk, Springer, Switzerland.

Lallemant, D., Kiremidjian, A. and Burton, H. (2015), "Statistical procedures for developing earthquake damage fragility curves", *Earthq. Eng. Struc. Dyn.*, **44**(9), 1373-1389. https://doi.org/10.1002/eqe.2522.

Liu, Y., Yu, X., Lu, D. and Ma, F. (2018), "Impact of initial damage path and spectral shape on aftershock collapse fragility of RC frames", *Earthq. Struct.*, **15**(5), 529-540. https://doi.org/10.12989/eas.2018.15.5.529.

Mengi, Y., McNiven, H.D. and Tanrikulu, A.K. (1992), "Models for nonlinear earthquake analysis of brick masonry buildings", Technical Report UCB-EERC 92/03, Earthquake Engineering and Research Center, University of California, California, U.S.A.

Motazedian, D. and Atkinson, G.M. (2005), "Stochastic finite-fault modeling based on a dynamic corner frequency", *Bull. Seismol. Soc. Am.*, **95**(3), 995-1010. https://doi.org/10.1785/0120030207.

Olsson, A., Sandberg, G. and Dahlblom, O. (2003), "On Latin hypercube sampling for structural reliability analysis", *Struct. Saf.*, **25**(1), 47-68. https://doi.org/10.1016/S0167-4730(02)00039-5.

OpenSees (2017), Open System for Earthquake Engineering Simulation Software Version 2.4.5, University of California, Berkeley, CA, U.S.A. http://opensees.berkeley.edu.

Park J.H. (2013), "Seismic response of SDOF systems representing masonry-infilled RC frames with damping systems", *Eng. Struct.*, **56**, 1735-1750. https://doi.org/10.1016/j.engstruct.2013.07.039.

Park, J., Towashiraporn, P., Craig, J.I. and Goodno, B.J. (2009), "Seismic fragility analysis of low-rise unreinforced masonry structures", *Eng. Struct.*, **31**(1), 125-137. https://doi.org/10.1016/j.engstruct.2008.07.021.

Rota M., Penna, A. and Magenes G. (2010), "A methodology for deriving analytical fragility curves for masonry buildings based on stochastic nonlinear analyses", *Eng. Struct.*, **32**(5), 1312-1323. https://doi.org/10.1016/j.engstruct.2010.01.009.

Sengezer, B.S. (1993), "The damage distribution during March 13, 1992 Erzincan Earthquake", *Proceedings of the 2nd National Earthquake Engineering Conference*, Turkey.

Sfahani, M.G. and Guan, H. (2018), "An extended cloud analysis method for seismic fragility assessment of highway bridges", *Earthq. Struct.*, **15**(6), 605-616. https://doi.org/10.12989/eas.2018.15.6.605.

Shinozuka, M., Feng, M.Q., Kim, H.K. and Kim, S.H. (2000), "Nonlinear static procedure for fragility curve development", *J. Eng. Mech.*, **126**(12), 1267-1295. https://doi.org/10.1061/(ASCE)0733-9399(2000)126:12(1287).

Simões, A., Milošević, J., Meireles, H., Bento, R., Cattari, S. and Lagomarsino, S. (2015), "Fragility curves for old masonry building types in Lisbon", *Bull. Earthq. Eng.*, **13**(10), 3083-3105. https://doi.org/10.1007/s10518-015-9750-1.

Sisi, A.A., Erberik, M.A. and Askan, A. (2018), "The effect of structural variability and local site conditions on building fragility functions", *Earthq. Struct.*, **14**(4), 285-295. https://doi.org/10.12989/eas.2018.14.4.285.

Sivaselvan, M.V. and Reinhorn, A.M. (1999), "Hysteretic models for cyclic behavior of deteriorating inelastic structures", Report

No. MCEER-99-0018, State University of New York, N.Y. U.S.A.
Snoj, J. and Dolšek, M. (2017), "Fragility functions for unreinforced masonry walls made from hollow clay units", *Eng*. *Struct*., **145**(15), 293-304. https://doi.org/10.1016/j.engstruct.2017.05.001.
Sokolov, V. and Zahran, H.M. (2018), "Generation of stochastic earthquake ground motion in western Saudi Arabia as a first step in development of regional ground motion prediction model", *Arab*. *J*. *Geosci*. *J*., **11**(38), 1866-7511. https://doi.org/10.1007/s12517-018-3394-9.
Sørensen, M.B. and Lang, D.H. (2015), "Incorporating simulated ground motion in seismic risk assessment-application to the Lower Indian Himalayas", *Earthq*. *Spectra*, **31**(1), 71-95. https://doi.org/10.1193%2F010412EQS001M.
Stojadinovic, B. and Thewalt, C.R. (1996). "Energy balanced hysteresis models", *Eleventh World Conference on Earthquake Engineering*, Paper No. 1734, Acapulco, Mexico.
Sucuoglu, H. and Erberik, M.A. (2004), "Energy based hysteresis and damage models for deteriorating systems", *Earthq*. *Eng*. *Struc*. *Dyn*., **33**(1), 69-88. https://doi.org/10.1002/eqe.338.
Sucuoglu, H. and Tokyay, M. (1992), "13 Mart 1992 Erzincan earthquake engineering report", Civil Engineering Department, Ankara.
Sun, J., Yu, Y. and Li, Y. (2018), "Stochastic finite-fault simulation of the 2017 Jiuzhaigou earthquake in China", *Earth Plan. Space*, **70**(1), 128. https://doi.org/10.1186/s40623-018-0897-2.
Takeda, T., Sozen, M. and Nielsen, N. (1970), "Reinforced concrete response to simulated earthquakes", *J. Struct*. *Div*., **96**(12), 2557-2573.
TUIK (2017), www.tuik.gov.tr/Web2013/iletisim/iletisim.html
Ugurhan, B. and Askan, A. (2010), "Stochastic strong ground motion simulation of the 12 November 1999 Duzce (Turkey) Earthquake using a dynamic corner frequency approach", *Bull*. *Seismol*. *Soc*. *Am*., **100**(4), 1498-1512. https://doi.org/10.1785/0120090358.
Ugurhan, B., Askan, A. and Erberik, M.A. (2011), "A methodology for seismic loss estimation in urban regions based on ground-motion simulations", *Bull*. *Seismol*. *Soc*. *Am*., **101**, 710-725. https://doi.org/10.1785/0120100159.
Utkucu, M., Nalbant, S.S., McCloskey, J., Steacy, S. and Alptekin, O. (2003), "Slip distribution and stress changes associated with the 1999 November 12, Duzce (Turkey) earthquake (*Mw*=7.1)", *Geophys*. *J*. *Int*., **153**, 229-241. https://doi.org/10.1046/j.1365-246X.2003.01904.x.
Whitman, R.V. (1973), "Damage probability matrices for prototype buildings", Report No. 380, Structures Publication, MIT, Boston, U.S.A.

CC